Controllable nonlinearity in a dual-coupling optomechanical system under a weak-coupling regime

Gui-Lei Zhu, Xin-You Lü,[*] Liang-Liang Wan, Tai-Shuang Yin, Qian Bin, and Ying Wu[†]

School of physics, Huazhong University of Science and Technology, Wuhan 430074, China

Strong quantum nonlinearity gives rise to many interesting quantum effects and has wide applications in quantum physics. Here we investigate the quantum nonlinear effect of an optomechanical system (OMS) consisting of both linear and quadratic coupling. Interestingly, a controllable optomechanical nonlinearity is obtained by applying a driving laser into the cavity. This controllable optomechanical nonlinearity can be enhanced into a strong coupling regime, even if the system is initially in the weak-coupling regime. Moreover, the system dissipation can be suppressed effectively, which allows the appearance of phonon sideband and photon blockade effects in the weak-coupling regime. This work may inspire the exploration of a dual-coupling optomechanical system as well as its applications in modern quantum science.

I. INTRODUCTION

Cavity optomechanics, exploring the nonlinear photon-phonon interaction via radiation pressure [1,2], has achieved tremendous advances in recent years, including the realization of cooling a macroscopic mechanical resonator to ground state [3–6], optomechanically induced transparency [7–10], coherent state conversion between cavity and mechanical modes [11–13], and the generation of squeezed light [14–16]. Those achievements offer the basic of exploring the applications of optomechanical nonlinearity which can be applied into quantum optics and quantum information sciences. In particular, recent studies have shown that the strong optomechanical nonlinearity could be used to generate single photon sources [17–20], engineer a nonclassical phonon state [21–24], and implement quantum information processing [25]. However, the strong nonlinearity is difficult to realize in a normal optomechanical system due to its weak photon-phonon interaction [1,2].

Recently, many methods have been proposed to enhance the radiation-pressure optomechanical coupling, such as using the photon hopping effects in two cavity systems [25–27] or multimode systems [28–31], Josephson effect in superconducting circuits [32–34], and the optical [35,36] and mechanical parameter amplification [37,38]. In previous proposals, only the linear optomechanical coupling is considered and an additional subsystem is needed to be introduced into the OMS, which limits its applications in the optomechanical many-body lattices [39–41].

Different from former works, here we investigate the optomechanical nonlinearity in an optomechanical system (OMS) with a membrane-in-the-middle configuration [42–44] [see Fig. 1(a)], including both the linear and quadratic optomechanical coupling. Specifically, the mechanical mode oscillates around the antinode and node of the resonator mode a_1 and a_2, respectively. Typically, the quadratic coupling is

much smaller than the linear coupling [45–49], which has been considered in the following discussion.

Interestingly, we found that a controllable optomechanical nonlinearity could be obtained without introducing an additional subsystem. Physically, by strong driving the linear mode a_1, two effective polariton modes with controllable frequencies are obtained. They couple to the quadratic mode a_2 with the form of radiation pressure, and have the controllable interaction strengths and coupling weights. This ultimately leads to the results that the strong radiation-pressure coupling can be obtained in an initially weakly coupled OMS. Moreover, the present optomechanical nonlinearity can be controlled easily, i.e., adjusting the frequency or strength of the driving laser. To show this controllable nonlinearity, the controllable phonon sidebands and photon blockade effects are demonstrated in the weak-coupling regime. This work is general and may also be applied into the photonic crystals [50–52] and microtoroidal resonator [53–55], even superconducting circuits with the ability of implementing quadratic interaction [56–58]. It effectively associates the linear and quadratic optomechanical interactions in a same OMS, which is interesting in broadening the regimes of cavity optomechanics as well as its applications in modern quantum technologies.

This paper is organized as follows: In Sec. II we introduce our model. The master equation describing the system's evolution and the controllable optomechanical nonlinearity of the proposed system are presented in Sec. III. In Sec. IV we discuss the nonlinear properties of this system featured by phonon sideband and photon blockade effects in the weak-coupling regime. In Sec. V we discuss the experimental prospect of our proposal. Finally, we conclude our results in Sec. VI. In addition, we provide a detailed derivation on the effective thermal occupancies in the Appendix.

II. THE MODEL

It is known that the optomechanical coupling between the optical cavity mode and the mechanical mode of an OMS

---

*xinyoulu@hust.edu.cn

†yingwu2@126.com
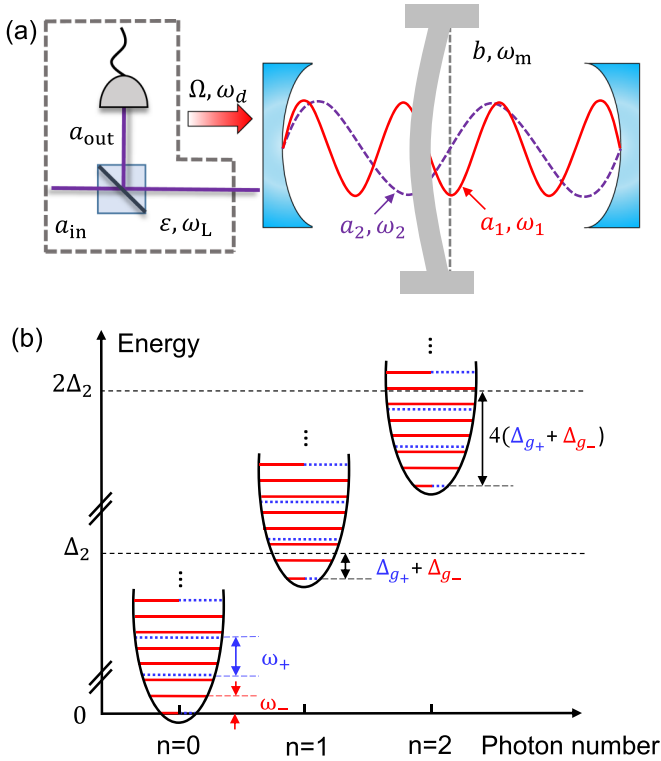
FIG. 1. (a) Schematic of a Fabry-Perot-type optomechanical system with a "membrane-in-the-middle" configuration, consisting of two optical cavity modes a_1 and a_2 coupled to the mechanical mode b. The driving field on cavity mode a_1 is described by amplitude Ω and frequency ω_d. A weak probe field (enclosed by the dashed lines) with frequency ω_L and amplitude ε is applied to detect the nonlinear optomechanical system. (b) The eigenvalues of the effective Hamiltonian H_{OMS}. Here the red solid lines represent the energy level of B_- mode while the blue dotted lines show the energy level of B_+. The parameters $\Delta_{g_\pm} = g_\pm^2/\omega_\pm$ are the energy shift of polariton modes $B_\pm$.

depends strongly on the position of the middle mirror (or membrane) [44]. When the mirror is placed in the vicinity of the antinodes of one cavity mode, the maximum coupling between the cavity mode and mechanical mode is linear, in that quadratic coupling and higher order coupling terms are much smaller than the linear one and can be ignored safely. The other case is that the mirror is put around nodes of a cavity mode, the linear coupling is near zero, accordingly, the maximum optomechanical coupling becomes quadratic.

Given the above, here we consider a Fabry-Perot-type optomechanical cavity system with a "membrane-in-the-middle" configuration, in which the mechanical mode (with frequency ω_m) couples to both the cavity mode a_1 (with frequency ω_1) linearly and a_2 (with frequency ω_2) quadratically, as shown in Fig. 1(a). Specifically, the mechanical mode oscillates around the antinodes and nodes of mode a_1 and a_2, respectively. This dual-coupling optomechanical device is applicable to trap and cool the partially reflective mirrors driven by bichromatic lasers [44,59].

In a frame rotating with frequency ω_d, the Hamiltonian of the optomechanical system depicted in Fig. 1(a) can be written

as ($\hbar = 1$)

$$H_{tot} = \delta_1 a_1^\dagger a_1 - g_1 a_1^\dagger a_1(b + b^\dagger) + \omega_2 a_2^\dagger a_2$$
$$- g_2 a_2^\dagger a_2(b + b^\dagger)^2 + \omega_m b^\dagger b + i\Omega(a_1^\dagger - a_1), \quad (1)$$

where a_1 (a_2) and b are the annihilation operators of the optical cavity modes and the mechanical mode, and g_1 (g_2) is the linear (quadratic) coupling strength between cavity mode a_1 (a_2) and mechanical mode b. Here Ω represents the laser driving strength and $\delta_1 = \omega_1 - \omega_d$ is the frequency detuning of the optical cavity from the driving field. When a strong red-detuning driving field is applied, the cavity could generate large steady-state amplitudes in both the cavity and the mechanical modes. We assume α_1 (β) is the steady-state amplitude of the cavity (mechanical) mode under the red-detuning driving. By using the displacement $a_1 \to a_1 + \alpha_1$, $b \to b + \beta$, the system Hamiltonian H_{tot} can be replaced by a shifted optomechanical Hamiltonian $H_{shifted} = H_{eff} + H_{nl}$ given by

$$H_{eff} = \Delta_1 a_1^\dagger a_1 + \Delta_2 a_2^\dagger a_2 - G_2 a_2^\dagger a_2(b + b^\dagger)$$
$$- G_1(a_1^\dagger + a_1)(b + b^\dagger) + \omega_m b^\dagger b, \quad (2a)$$
$$H_{nl} = -g_1 a_1^\dagger a_1(b + b^\dagger) - g_2 a_2^\dagger a_2(b + b^\dagger)^2. \quad (2b)$$

Here G_1 is the linearized optomechanical coupling strength, G_2 is the radiation-pressure coupling strength, and Δ_1, Δ_2 are the shifted detuning, given by

$$\Delta_1 = \delta_1 - 2g_1\beta, \quad \Delta_2 = \omega_2 - 4g_2\beta^2, \quad (3a)$$
$$G_1 = g_1|\alpha_1|, \quad G_2 = 4g_2|\beta|. \quad (3b)$$

The steady-state mean values α_1, β satisfy $\omega_m\beta - g_1|\alpha_1|^2 = 0$. Without loss of generality, we have taken $\alpha_1, \beta, G_1, G_2$ to be real and positive. Under the condition of $G_1, G_2 \gg g_1, g_2$, the Hamiltonian H_{nl} can be ignored safely in our following calculations.

From Eq. (3b) we found that the introduced radiation-pressure coupling strength G_2 is proportional to the mechanical displacement β. In the following we will give a simple analytical derivation to clarify this effect; provided that the equilibrium position of membrane is effectively shifted with amplitude β, i.e., $b \to b + \beta$. Accordingly, we could obtain $g_2 a_2^\dagger a_2(b + b^\dagger + 2\beta)^2 = g_2 a_2^\dagger a_2(b + b^\dagger)^2 + G_2 a_2^\dagger a_2(b + b^\dagger) + 4\beta^2 g_2 a_2^\dagger a_2$. As is shown in this equation, first, the steady-state displacement of membrane cannot enhance the originally quadratic coupling strength g_2. Second, a radiation-pressure coupling is introduced, and its strength G_2 is proportional to the displacement β. The last term $4\beta^2 g_2 a_2^\dagger a_2$ merely changes the cavity's resonant frequency.

Physically, we could understand this effect as following. In our proposal, a strong driving field applied to cavity mode a_1 changes the effective equilibrium position of membrane, i.e., the membrane deviates from the nodes of a_2 mode. This shift introduces a radiation-pressure optomechanical coupling from the original quadratic optomechanical interaction. Then the dominated optomechanical coupling shifts from quadratic form [i.e., four-operators term $a_2^\dagger a_2(b + b^\dagger)^2$] to a radiation-pressure form [i.e., three-operators term $a_2^\dagger a_2(b + b^\dagger)$], in that the strength of the introduced radiation-pressure coupling is

enhanced by the displacement amplitude β of membrane's equilibrium position. Actually, this process is similar to the linearization procedure [60–63], i.e., when a strong driving field is applied to a normal OMS with radiation-pressure coupling $g_0 a^\dagger a (b + b^\dagger)$, the dominated optomechanical interaction will shift from the radiation-pressure coupling to a linearized optomechanical interaction $G(a + a^\dagger)(b + b^\dagger)$. Because the linearized optomechanical coupling strength $G = g_0 \alpha$ ($|\alpha|^2$ is the mean photon number in the cavity) can be much larger than g_0.

III. CONTROLLABLE OPTOMECHANICAL NONLINEARITY

Interestingly, the present system has a controllable optomechanical interaction, which leads to the controllable optomechanical nonlinearity. Specifically, Eq. (2a) can be diagonalized via a Bogoliubov transformation $R = MB$ with $R^T = (a_1, a_1^\dagger, b, b^\dagger)$ and $B^T = (B_-, B_-^\dagger, B_+, B_+^\dagger)$. We refer to $B_\pm$ as polariton modes including both photonic and phononic components, and the transformation matrix is given by [24]

$$M = \begin{pmatrix} C_+ & C_- & D_+ & D_- \\ C_- & C_+ & D_- & D_+ \\ -E_+ & -E_- & F_+ & F_- \\ -E_- & -E_+ & F_- & F_+ \end{pmatrix}, \quad (4)$$

where the matrix factors $C_\pm, D_\pm, E_\pm, F_\pm$ read

$$C_\pm = \frac{\cos\theta}{2} \frac{(\Delta_1 \pm \omega_-)}{\sqrt{\Delta_1 \omega_-}}, \quad D_\pm = \frac{\sin\theta}{2} \frac{(\Delta_1 \pm \omega_+)}{\sqrt{\Delta_1 \omega_+}}, \quad (5a)$$

$$E_\pm = \frac{\sin\theta}{2} \frac{(\omega_m \pm \omega_-)}{\sqrt{\omega_m \omega_-}}, \quad F_\pm = \frac{\cos\theta}{2} \frac{(\omega_m \pm \omega_+)}{\sqrt{\omega_m \omega_+}}. \quad (5b)$$

By using the inverse of matrix M, we obtain the expression of new mode $B_\pm$ in terms of a_1 and b modes, i.e.,

$$B_- = C_+ a_1 - C_- a_1^\dagger - E_+ b + E_- b^\dagger, \quad (6a)$$

$$B_-^\dagger = -C_- a_1 + C_+ a_1^\dagger + E_- b - E_+ b^\dagger, \quad (6b)$$

$$B_+ = D_+ a_1 - D_- a_1^\dagger + F_+ b - F_- b^\dagger, \quad (6c)$$

$$B_+^\dagger = -D_- a_1 + D_+ a_1^\dagger - F_- b + F_+ b^\dagger. \quad (6d)$$

After a Bogoliubov transformation, we obtain a standardlike optomechanical Hamiltonian, given by

$$\begin{aligned} H_{\text{OMS}} = {} & \Delta_2 a_2^\dagger a_2 + \omega_+ B_+^\dagger B_+ - g_+ a_2^\dagger a_2 (B_+ + B_+^\dagger) \\ & + \omega_- B_-^\dagger B_- - g_- a_2^\dagger a_2 (B_- + B_-^\dagger). \end{aligned} \quad (7)$$

Here $\omega_\pm$ are the polariton mode frequencies of the subsystem,

$$\omega_\pm^2 = \frac{1}{2}\left(\Delta_1^2 + \omega_m^2 \pm \sqrt{(\omega_m^2 - \Delta_1^2)^2 + 16 G_1^2 \Delta_1 \omega_m}\right) \quad (8)$$

and the effective coupling strengths of the optomechanical subsystem are given by

$$g_- = -4 g_2 \beta \sin\theta \sqrt{\frac{\omega_m}{\omega_-}}, \quad (9a)$$

$$g_+ = +4 g_2 \beta \cos\theta \sqrt{\frac{\omega_m}{\omega_+}}, \quad (9b)$$
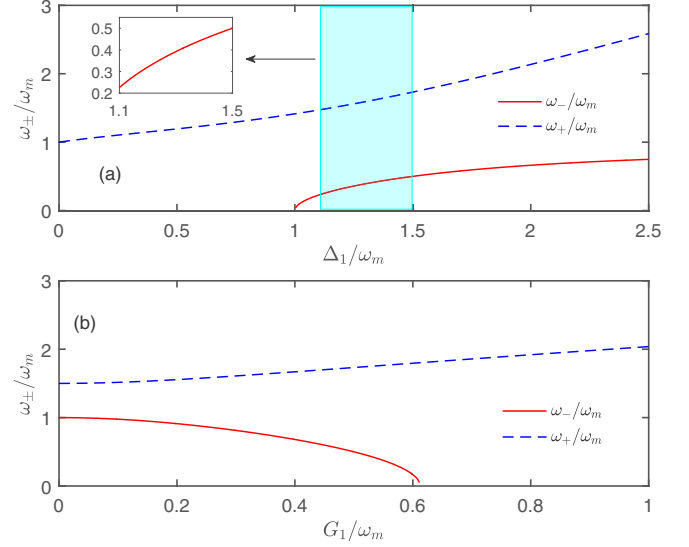
FIG. 2. The polariton modes $\omega_\pm$ of the optomechanical subsystem. Plots of the relationship between $\omega_\pm$ and (a) detuning Δ_1/ω_m, (b) the linearized coupling strength G_1/ω_m. Main parameters including $\beta = 25$, $g_1/\omega_m = 10^{-2}$, in (b) $\delta_1/\omega_m = 2.0$. The shadowed area indicates the considered parameter range in our proposal.

with the angle θ defined as

$$\tan 2\theta = \frac{4 G_1 \sqrt{\Delta_1 \omega_m}}{\Delta_1^2 - \omega_m^2}. \quad (10)$$

From Eqs. (6) we could obtain polariton modes $B_\pm$ of optical and mechanical modes. As discussed in Sec. II, the introduced radiation-pressure coupling strength G_2 could be enhanced by the displacement amplitude β. Moreover, as is shown in Eq. (9a), the effective subsystem's radiation-pressure coupling strength g_- can be enhanced when the polariton mode frequency ω_- is decreased. Physically, this result can be understood as following. When the polariton mode frequency ω_- decreases, the polariton mode B_- coupled to the optical field is highly softened. Accordingly, the subsystem's radiation-pressure coupling g_- is largely enhanced. In addition, in the extreme case of $\omega_- \to 0$, g_- approaches infinity. However, in our proposal, the considered region is far from $\omega_- = 0$, which avoids the appearance of this singular point.

Specifically, Eq. (8) shows that $G_1 = \sqrt{\Delta_1 \omega_m}/2$ corresponds to a critical point of $\omega_-^2 = 0$. Theoretically, when $\omega_- \to 0$, the matrix factors C, D, E, F approach infinity, then the new modes $B_\pm$ tend to be zero (zero combinations of mode a_1 and b). However, in our proposal, we have taken the value of Δ_1 from $1.1\omega_m$ to $1.5\omega_m$, accordingly ω_- ranges from $0.25\omega_m$ to $0.5\omega_m$. As shown in the inset of Fig. 2(a), the chosen parameter region of ω_- is far away from the critical point $\omega_- = 0$. In order to make it more explicit, we plotted the function of matrix factors C, D, E, F versus detuning Δ_1/ω_m in Fig. 3. It is shown that, in the considered parameter region, the matrix factors C, D, E, F are finite, which ensures the validity of polariton mode B_-.

In Fig. 4 we present the dependence of the effective coupling strength $g_\pm$ on system parameters Δ_1 and G_1. It is shown
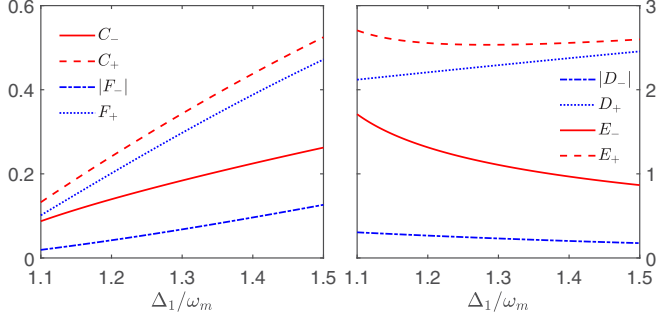
FIG. 3. The values of matrix factors $C, |D|, E, |F|$ versus detuning Δ_1/ω_m corresponding to the region of Fig. 2. The parameters are chosen as $\beta = 25$, $g_1/\omega_m = 10^{-2}$.

that, in the considered region, g_- can be enhanced. Together with the validity of the polariton mode B_-, the enhancement of system nonlinearity decided by increasing g_- has real meaning. Moreover, here the optical mode couples to the two effective polariton modes with a weight decided by θ. As shown in Fig. 5, θ ranges from 0 to 0.75 and also can be controlled by modulating the detuning Δ_1/ω_m. By adjusting the driving laser applied into mode a_1, the proposed system has a controllable optomechanical nonlinearity decided by the controllable optomechanical interactions.

IV. PHONON SIDEBAND AND PHOTON BLOCKADE EFFECT IN THE WEAK-COUPLING REGIME

Generally speaking, the strong optomechanical nonlinearity can induce a phonon sideband in the excitation spectrum and a photon blockade under the condition of a weak driving field. In order to probe (or utilize) this controllable nonlinearity, we drive the cavity mode a_2 using a weak probe field with frequency ω_L, amplitude ε ($\varepsilon \ll \kappa$), where κ is the initial cavity
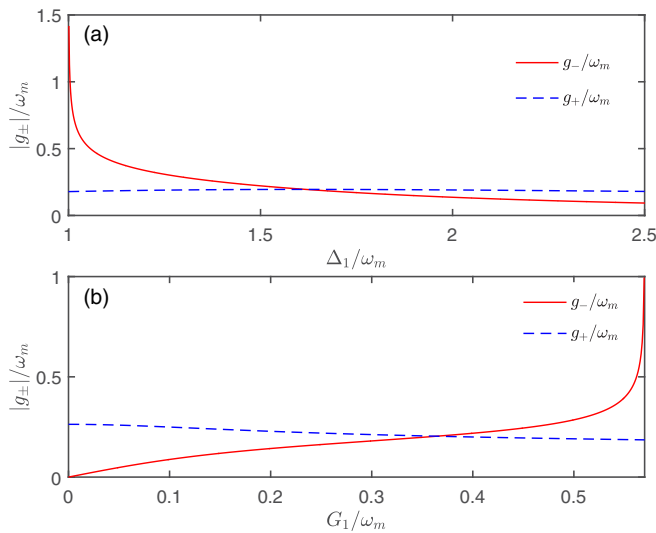
FIG. 4. The effective coupling strengths versus (a) the detuning Δ_1/ω_m and (b) the linearized coupling strength G_1/ω_m. The system parameters are $\delta_1/\omega_m = 1.80$ for (a), other parameters are chosen as $\beta = 25$, $g_1/\omega_m = 10^{-2}$, $g_2/\omega_m = 3 \times 10^{-3}$.
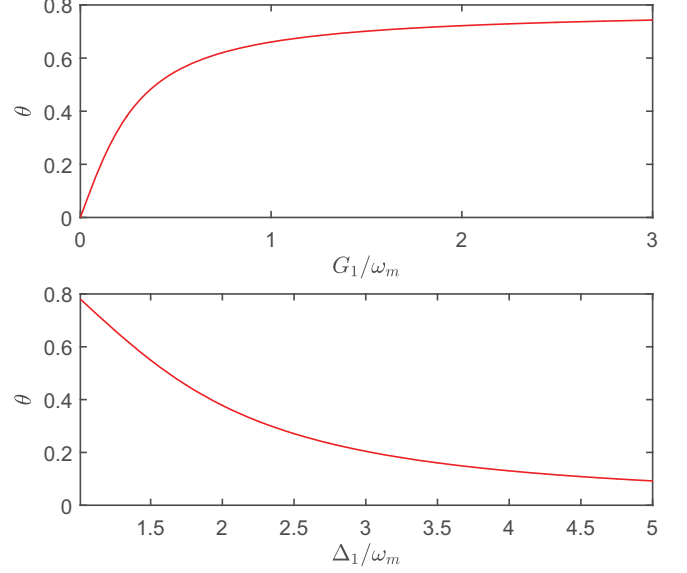
FIG. 5. Relationship between angle θ and linearized coupling strength G_1/ω_m and the detuning Δ_1/ω_m. The parameters are $\beta = 25$, $g_1/\omega_m = 10^{-2}$, and $\delta_1/\omega_m = 2.0$.

damping rate. Then the effective system Hamiltonian becomes

$$H'_{\text{OMS}} = \Delta'_2 a_2^\dagger a_2 + \sum_{\sigma=\pm} \omega_\sigma B_\sigma^\dagger B_\sigma$$
$$- \sum_{\sigma=\pm} g_\sigma a_2^\dagger a_2 (B_\sigma + B_\sigma^\dagger) + i\varepsilon(a_2^\dagger - a_2), \quad (11)$$

where $\Delta'_2 = \Delta_2 - \omega_L$. By diagonalizing H'_{OMS} with the transformation $H'_{\text{OMS}} \to U H'_{\text{OMS}} U$ and $U = e^{-iP a_2^\dagger a_2}$, $P = i \sum_\sigma (\frac{g_\sigma}{\omega_\sigma})(B_\sigma^\dagger - B_\sigma)$, we can obtain

$$H'_{\text{OMS}} = \Delta'_2 a_2^\dagger a_2 + \sum_\sigma \left(\omega_\sigma B_\sigma^\dagger B_\sigma - \frac{g_\sigma^2}{\omega_\sigma} a_2^\dagger a_2^\dagger a_2 a_2 \right)$$
$$+ i\varepsilon(a_2^\dagger e^{iP} - e^{-iP} a_2). \quad (12)$$

Then the system eigenstates are $|n, \tilde{m}_+, \tilde{m}_-\rangle$ and corresponding eigenvalues given by

$$E_{n,\tilde{m}_\sigma} = n\Delta_2 - \sum_\sigma \left(n^2 \frac{g_\sigma^2}{\omega_\sigma} - m_\sigma \omega_\sigma \right), \quad (13)$$

where n, m_σ are the non-negative integers and $|n, \tilde{m}_+, \tilde{m}_-\rangle = U|n, m_+, m_-\rangle$. Here $|n, m_+, m_-\rangle$ represents a state of n photons and m_σ polaritons.

The results mentioned above show that we obtain an optomechanical system with two effective polariton modes (i.e., $B_\pm$) coupled to a same cavity mode a_2. The corresponding coupling weight decided by θ can be controlled by tuning the frequency detuning δ_1. Qualitatively, we present the energy level structure of system in Fig. 1(b), which clearly shows the strong Kerr nonlinearity of system coming from both of the two optomechanical interactions between a_2 and $B_\pm$. Then, to show quantitatively the nonlinearity induced phonon sideband and photon blockade, we numerically calculate system dynamics including the cavity mode a_2 and two polariton modes $B_\pm$.
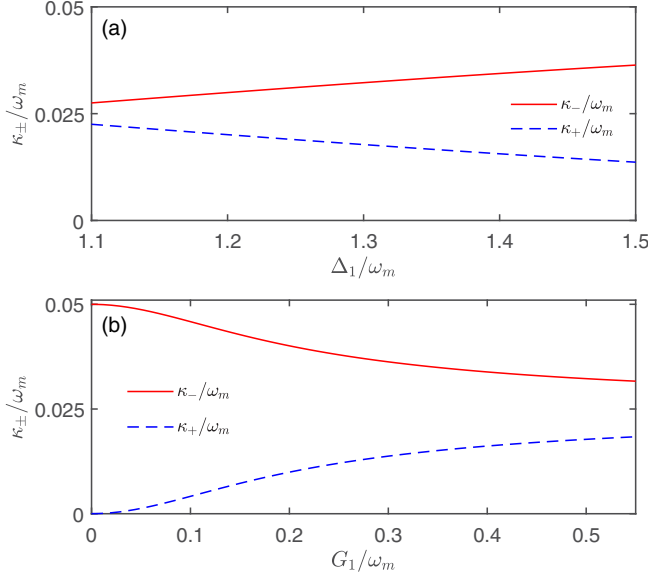
FIG. 6. The corresponding effective damping rates of the subsystem. Main parameters are $\beta = 25$, $g_1/\omega_m = 10^{-2}$, $\gamma/\omega_m = 10^{-5}$, $\kappa/\omega_m = 5 \times 10^{-2}$, and $\delta_1/\omega_m = 1.80$ for (b).

Particularly, within a Lindblad approach for the system dissipation, the system dynamics is decided by the master equation given by [64]

$$\frac{d\rho}{dt} = -i[H_{\mathrm{OMS}},\rho] + \kappa\mathcal{D}[a_2]\rho + \kappa_-\bar{n}_-\mathcal{D}[B_-^\dagger]\rho$$

$$+\kappa_-(\bar{n}_- + 1)\mathcal{D}[B_-]\rho + \kappa_+\bar{n}_+\mathcal{D}[B_+^\dagger]\rho$$

$$+\kappa_+(\bar{n}_+ + 1)\mathcal{D}[B_+]. \tag{14}$$

Here $\mathcal{D}[o]\rho = o\rho o^\dagger - (o^\dagger o\rho + \rho o^\dagger o)/2$ is the standard Lindblad superoperator for the damping of the polariton modes. The effective polariton damping rates $\kappa_\pm$ read

$$\kappa_- = \gamma\frac{\omega_m\sin^2\theta}{\omega_-} + \kappa\cos^2\theta, \tag{15a}$$

$$\kappa_+ = \gamma\frac{\omega_m\cos^2\theta}{\omega_+} + \kappa\sin^2\theta, \tag{15b}$$

where κ and γ are the initial cavity and mechanical damping rate, respectively. As one can see in Fig. 6, κ_+ decreases with increasing Δ_1/ω_m while κ_- becomes larger with increasing Δ_1/ω_m, but all $\kappa_\pm$ are smaller than initial cavity damping rate κ. Moreover, $\kappa_\pm$ have an inverse tendency with the growth of G_1/ω_m. In the region discussed in this paper, the corresponding damping rates of the subsystem can be suppressed effectively. We assume the mechanical bath to be at temperature $T_{\mathrm{M}} = 0$, then the effective thermal occupancies for modes $B_\pm$ can be written as

$$\bar{n}_- = \frac{\kappa\cos^2\theta}{4\kappa_-\Delta_1\omega_-}(\Delta_1 - \omega_-)^2, \tag{16a}$$

$$\bar{n}_+ = \frac{\kappa\sin^2\theta}{4\kappa_+\Delta_1\omega_+}(\Delta_1 - \omega_+)^2. \tag{16b}$$
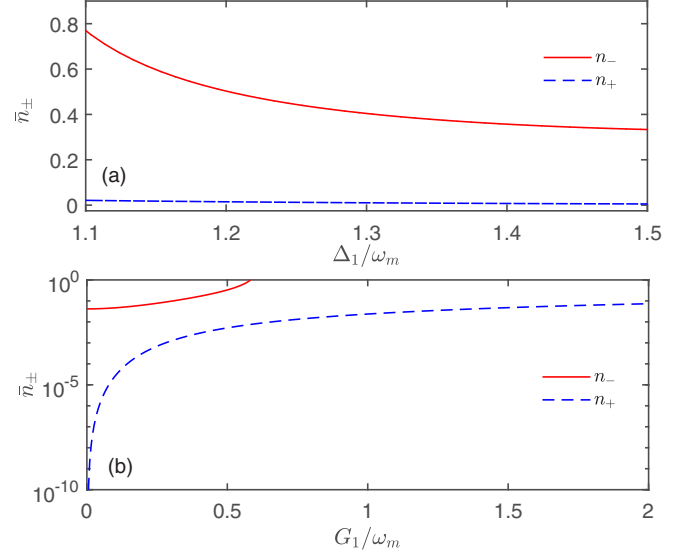
FIG. 7. The resulting effective bath thermal occupancies of the cavity and mechanical modes. Parameters are $\beta = 25$, $g_1/\omega_m = 10^{-2}$, $\gamma/\omega_m = 10^{-5}$, $\kappa/\omega_m = 5 \times 10^{-2}$, and $\delta_1/\omega_m = 2.0$ for (b).

Here $\bar{n}_\pm$ originally comes from the environments of the optical mode a_1 and mechanical mode b [see the definition of $B_\pm$ shown in Eqs. (6)]. The detailed derivation of Eqs. (16) is given in the Appendix. In Fig. 7 we plot the relationship between effective bath thermal occupancies given in Eqs. (16) and variables Δ_1/ω_m and G/ω_m. It is shown that, in the
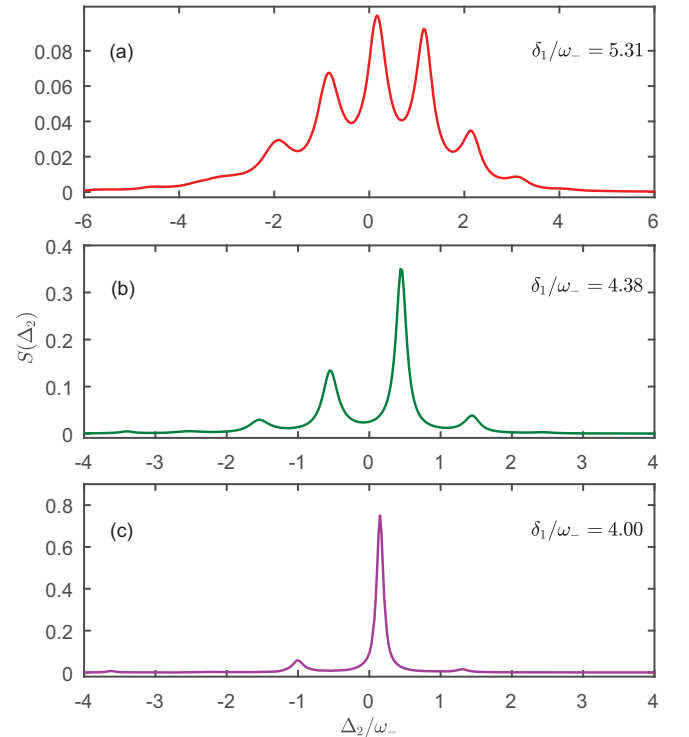
FIG. 8. Optical cavity output spectrum $S(\Delta_2)$ for three different values of the detuning δ_1/ω_-. (a) $\delta_1/\omega_- = 5.31$, $g_1/\omega_- = 3.00 \times 10^{-2}$, $g_2/\omega_- = 9.36 \times 10^{-3}$, (b) $\delta_1/\omega_- = 4.38$, $g_1/\omega_- = 2.37 \times 10^{-2}$, $g_2/\omega_- = 7.10 \times 10^{-3}$, and (c) $\delta_1/\omega_- = 4.00$, $g_1/\omega_- = 2.00 \times 10^{-2}$, $g_2/\omega_- = 6.00 \times 10^{-3}$.
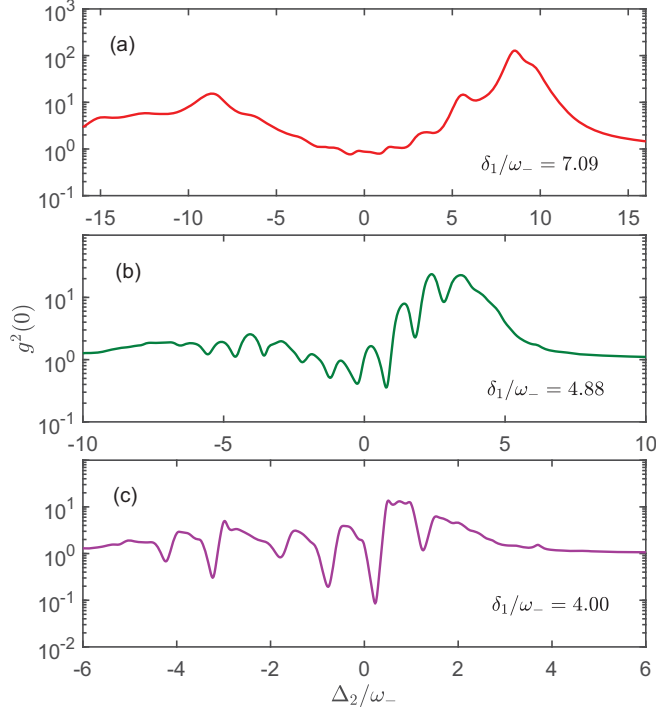
FIG. 9. The equal-time second-order correlation function $g^2(0)$ versus the driving detuning Δ_2/ω_- for various values of the detuning δ_1/ω_- for (a) $\delta_1/\omega_- = 7.09$, $g_1/\omega_- = 4.43 \times 10^{-2}$, $g_2/\omega_- = 1.33 \times 10^{-2}$, (b) $\delta_1/\omega_- = 4.88$, $g_1/\omega_- = 2.80 \times 10^{-2}$, $g_2/\omega_- = 8.37 \times 10^{-3}$, and (c) $\delta_1/\omega_- = 4.00$, $g_1/\omega_- = 2.00 \times 10^{-2}$, $g_2/\omega_- = 6.00 \times 10^{-3}$.

considered region, $n_\pm$ are all less than 0.8, which ultimately ensures the probability to observe phonon sidebands and photon blockade effects in our proposal.

To demonstrate the phonon sideband, we calculate the steady-state excitation spectrum

$$S(\Delta_2) = \lim_{t \to \infty} \frac{\langle a_2^\dagger a_2 \rangle(t)}{n_0}, \qquad (17)$$

where the resonant photon number $n_0 = 4\varepsilon^2/\kappa^2$. By using Eq. (17) with Hamiltonian H_{OMS}, we plot the optical photon excitation spectrum $S(\Delta_2)$ as a function of various detuning δ_1/ω_- in Fig. 8. (Note that we plot Figs. 8, 9, and 10 [65] using the Hamiltonian H_{OMS} and considering three modes, i.e., a_2, B_+, and B_-.) It shows that the phonon sideband appears in the originally weak-coupling regime and also can be controlled by the detuning δ_1/ω_-. This clearly demonstrates the controllable optomechanical nonlinearity featured in our system, which could effectively enter into the strong coupling regime, i.e., $g_\pm > \kappa_\pm$.

To demonstrate the photon blockade effect, we calculate the equal-time second-order correlation function in a steady state

$$g^{(2)}(0) = \lim_{t \to 0} \frac{\langle a_2^\dagger a_2^\dagger a_2 a_2 \rangle(t)}{\langle a_2^\dagger a_2 \rangle^2(t)}. \qquad (18)$$

By numerically solving Eq. (18) with Hamiltonian H_{OMS}, accordingly, the second-order correlation function $g^2(0)$ of the optomechanical system can be calculated. In Figs. 9 and 10 we illustrate the dependence of $g^2(0)$ on the weak probe field
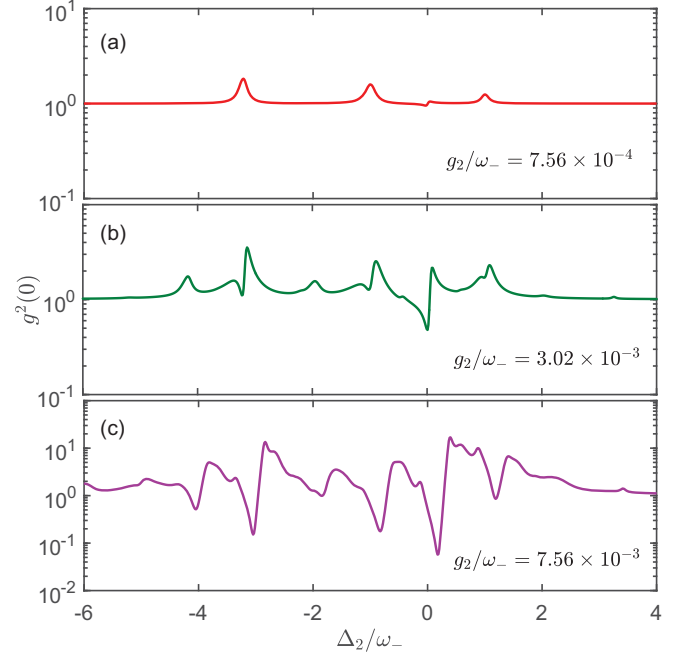
FIG. 10. The equal-time second-order correlation function $g^2(0)$ versus the driving detuning Δ_2/ω_- for various values of the quadratic coupling strength g_2/ω_-. Parameters are $\beta = 25$, $g_1/\omega_- = 1.51 \times 10^{-2}$, $\delta_1/\omega_- = 3.78$ and (a) $g_2/\omega_- = 7.56 \times 10^{-4}$, (b) $g_2/\omega_- = 3.02 \times 10^{-3}$, and (c) $g_2/\omega_- = 7.56 \times 10^{-3}$.

detuning Δ_2/ω_- for different driving detuning δ_1/ω_- and initial quadratic coupling strength g_2/ω_-.

Figure 9(a) shows that there is no photon blockade [$g^2(0) \ll 1$] for large detuning δ_1/ω_- since large detuning causes weak nonlinearity and large effective bath thermal occupancies $n_\pm$. With the decrease of δ_1/ω_-, we observe a series of bunching (peaks) and antibunching (dips) resonances with the change of Δ_2/ω_-. This indicates that the nonlinear effect is enhanced extensively and the noise of the optomechanical system is suppressed effectively along with the decrease of driving detuning δ_1/ω_-. When $\delta_1/\omega_- \leqslant 4.00$, the photon blockade effect appears in certain values of Δ_2/ω_- due to the system effectively reaching into the strong-coupling regime [see Fig. 9(c)]. Again, these results also demonstrate that the controllable optomechanical nonlinearity can be realized in our proposal. In Fig. 10 we plot the second-order equal time correlation function $g^2(0)$ as a function of Δ_2/ω_- when the initial quadratic coupling strength g_2 takes various values. It is also clearly shown that the realization of a photon blockade in the weak-coupling regime is based on our proposal. In other words, the strong optomechanical nonlinearity could be realized in the weakly coupled OMS.

V. DISCUSSIONS

In this section we discuss the experimental feasibility of our proposal. To obtain a strong linearized interaction between the optical mode a_1 and mechanical mode b (i.e., $G_1 = \alpha_1 g_1 \sim 0.1\omega_m$), a large optomechanical interaction strength $g_1/\omega_m = 10^{-2}$ and cavity photon number $\langle a_1^\dagger a_1 \rangle = \alpha_1^2 = 2500$ have been chosen here. Until now, it is still challenging to

realize $g_1/\omega_m = 10^{-2}$ in the normal optomechanical system [1]. In principle, this problem can be solved by increasing the mean photon number $\langle a_1^\dagger a_1 \rangle$ with applying a strong driving laser. As shown in Ref. [4], the cavity photon number up to 10^{10} has been realized experimentally, which manifests that the restriction of the parameter condition g_1/ω_m of our proposal can be relaxed largely theoretically.

Moreover, a relatively strong optomechanical coupling strength $g_1/\omega_m \sim 10^{-2}$ has been obtained in the optomechanical crystal [50,66] or ultracold atomic optomechanical system [67]. Recently, many potential theoretical schemes have been proposed to enhance the single-photon optomechanical coupling strength by utilizing the Josephson effect in superconducting circuits [33], the squeezing effect [35,37], and so on. In a short summary, it might be still challenging to implement our proposal completely with current available experimental technology. We hope it will be realized in further experiments along with the progress of cavity optomechanics.

VI. CONCLUSION

In conclusion, we presented a method to obtain controllable optomechanical nonlinearity in an OMS including both the linear and quadratic optomechanical coupling. By applying a strong driving laser into a cavity, we have shown that the optomechanical coupling could be enhanced enormously without loss of the nonlinearity, i.e., from weak-coupling regime to an effective strong radiation-pressure coupling regime. To demonstrate the controllable optomechanical nonlinearity, we numerically calculated cavity excitation spectrum and second-order correlation function, and presented the appearances of phonon sidebands and photon blockade effects in the originally weak-coupling regime. Our results shown that, in the dual-coupling optomechanical system, one can easily enhance the optomechanical nonlinearity by applying a strong driving laser. This study provides a promising route to reach the strong nonlinear regime of an OMS with available technology, and has potential applications in modern quantum science.

ACKNOWLEDGMENTS

APPENDIX: DERIVATION OF THE EFFECTIVE THERMAL OCCUPANCIES

In this Appendix we show the detailed discussion on the generation of the effective thermal occupancies $\bar{n}_\pm$. Here $\bar{n}_\pm$ are the effective thermal occupancies of polariton modes B_+

and B_-. The initial master equation with Hamiltonian H_{eff} can be written as

$$\frac{d\rho}{dt} = -i[H_{\text{eff}}, \rho(t)] + \kappa \mathcal{D}[a_1]\rho + \kappa \mathcal{D}[a_2]\rho$$
$$+ (\bar{n}+1)\gamma \mathcal{D}[b]\rho + \bar{n}\gamma \mathcal{D}[b^\dagger]\rho, \quad \text{(A1)}$$

here $\mathcal{D}[o]\rho = o\rho o^\dagger - (o^\dagger o \rho + \rho o^\dagger o)/2$ is the standard Lindblad superoperator. $\bar{n} = \bar{n}_B[\omega_m, T_M] = [\exp(\omega_m/k_B T_M) - 1]^{-1}$ is the mean number of the mechanical mode inside the bath, k_B is the Boltzmann constant, and the mechanical bath is at temperature T_M. Applying the inverse of Eqs. (6a)–(6d) into Eq. (A1), we can then obtain the effective master equation [see Eq. (14)]. Accordingly, the effective polariton damping rates are [64]

$$\kappa_- = \gamma(E_+ + E_-)^2 + \kappa(C_+^2 - C_-^2)$$
$$= \gamma \frac{\omega_m \sin^2\theta}{\omega_-} + \kappa \cos^2\theta, \quad \text{(A2a)}$$

$$\kappa_+ = \gamma(F_+ + F_-)^2 + \kappa(D_+^2 - D_-^2)$$
$$= \gamma \frac{\omega_m \cos^2\theta}{\omega_+} + \kappa \sin^2\theta, \quad \text{(A2b)}$$

where C, D, E, F are matrix factors of Eqs. (5). Specifically, when the initial modes a_1 and b transform into polariton modes B_+ and B_-, the interaction between cavity and bath generates nonconserving terms and these nonconserving terms lead to polariton heating. The thermal occupancies read

$$\bar{n}_- = \frac{1}{\kappa_-}[\gamma(E_+ + E_-)^2 \bar{n}_B[\omega_-, T_M] + \kappa C_-^2]$$
$$= \frac{\gamma \omega_m \sin^2\theta}{\kappa_- \omega_-} \bar{n}_B[\omega_-, T_M] + \frac{\kappa \cos^2\theta}{4\kappa_- \Delta_1 \omega_-}(\Delta_1 - \omega_-)^2, \quad \text{(A3a)}$$

$$\bar{n}_+ = \frac{1}{\kappa_+}[\gamma(F_+ + F_-)^2 \bar{n}_B[\omega_+, T_M] + \kappa D_-^2]$$
$$= \frac{\gamma \omega_m \cos^2\theta}{\kappa_+ \omega_+} \bar{n}_B[\omega_+, T_M] + \frac{\kappa \sin^2\theta}{4\kappa_+ \Delta_1 \omega_+}(\Delta_1 - \omega_+)^2. \quad \text{(A3b)}$$

We choose the temperature of the mechanical bath to be zero, i.e., $\bar{n}_B[\omega_-, T_M] = \bar{n}_B[\omega_+, T_M] = 0$, then we obtain the effective thermal occupancy as follows:

$$\bar{n}_- = \frac{\kappa \cos^2\theta}{4\kappa_- \Delta_1 \omega_-}(\Delta_1 - \omega_-)^2, \quad \text{(A4a)}$$

$$\bar{n}_+ = \frac{\kappa \sin^2\theta}{4\kappa_+ \Delta_1 \omega_+}(\Delta_1 - \omega_+)^2. \quad \text{(A4b)}$$

[1] M. Aspelmeyer, T. J. Kippenberg, and F. Marquardt, Rev. Mod. Phys. **86**, 1391 (2014); M. Aspelmeyer, P. Meystre, and K. Schwab, Phys. Today **65**(7), 29 (2012); P. Meystre, Ann. Phys. (Berlin) **525**, 215 (2013); T. J. Kippenberg and K. J. Vahala, Science **321**, 1172 (2008); F. Marquardt and S. M. Girvin, Physics **2**, 40 (2009).

[2] H. Xiong, L.-G. Si, X.-Y. Lü, X.-X. Yang, and Y. Wu, Sci. China: Phys. Mech. Astron. **58**, 1 (2015).

[3] A. D. O'Connell *et al.*, Nature (London) **464**, 697 (2010).

[4] S. Gröblacher, K. Hammerer, M. R. Vanner, and M. Aspelmeyer, Nature (London) **460**, 724 (2009).

[5] J. Chan, T. P. M. Alegre, A. H. Safavi-Naeini, J. T. Hill, A. Krause, S. Gröblacher, M. Aspelmeyer, and O. Painter, Nature (London) **478**, 89 (2011).

[6] J. D. Teufel, T. Donner, D. Li, J. W. Harlow, M. S. Allman, K. Cicak, A. J. Sirois, J. D. Whittaker, K. W. Lehnert, and R. W. Simmonds, Nature (London) **475**, 359 (2011).

[7] S. Weis, R. Rivière, S. Deléglise, E. Gavartin, O. Arcizet, A. Schliesser, and T. J. Kippenberg, Science **330**, 1520 (2010).

[8] A. H. Safavi-Naeini, T. P. Mayer Alegre, J. Chan, M. Eichenfield, M. Winger, Q. Lin, J. T. Hill, D. E. Chang, and O. Painter, Nature (London) **472**, 69 (2011).

[9] A. Kronwald and F. Marquardt, Phys. Rev. Lett. **111**, 133601 (2013).

[10] M. Karuza, C. Biancofiore, M. Bawaj, C. Molinelli, M. Galassi, R. Natali, P. Tombesi, G. Di Giuseppe, and D. Vitali, Phys. Rev. A **88**, 013804 (2013).

[11] V. Fiore, Y. Yang, M. C. Kuzyk, R. Barbour, L. Tian, and H. Wang, Phys. Rev. Lett. **107**, 133601 (2011).

[12] X. Zhou, F. Hocke, A. Schliesser, A. Marx, H. Huebl, R. Gross, and T. J. Kippenberg, Nat. Phys. **9**, 179 (2013).

[13] T. A. Palomaki, J. W. Harlow, J. D. Teufel, R. W. Simmonds, and K. W. Lehnert, Nature (London) **495**, 210 (2013); T. A. Palomaki, J. D. Teufel, R. W. Simmonds, and K. W. Lehnert, Science **342**, 710 (2013).

[14] D. W. C. Brooks, T. Botter, S. Schreppler, T. P. Purdy, N. Brahms, and D. M. Stamper-Kurn, Nature (London) **488**, 476 (2012).

[15] A. H. Safavi-Naeini, S. Gröblacher, J. T. Hill, J. Chan, M. Aspelmeyer, and O. Painter, Nature (London) **500**, 185 (2013).

[16] T. P. Purdy, P.-L. Yu, R. W. Peterson, N. S. Kampel, and C. A. Regal, Phys. Rev. X **3**, 031012 (2013).

[17] M. Keller, B. Lange, K. Hayasaka, W. Lange, and H. Walther, Nature (London) **431**, 1075 (2004).

[18] B. Lounis and W. E. Moerner, Nature (London) **407**, 491 (2000).

[19] P. Rabl, Phys. Rev. Lett. **107**, 063601 (2011).

[20] A. Nunnenkamp, K. Børkje, and S. M. Girvin, Phys. Rev. Lett. **107**, 063602 (2011).

[21] S. Bose, K. Jacobs, and P. L. Knight, Phys. Rev. A **56**, 4175 (1997).

[22] A. P. Lund, H. Jeong, T. C. Ralph, and M. S. Kim, Phys. Rev. A **70**, 020101(R) (2004).

[23] B. Pepper, R. Ghobadi, E. Jeffrey, C. Simon, and D. Bouwmeester, Phys. Rev. Lett. **109**, 023601 (2012).

[24] X.-Y. Lü, W.-M. Zhang, S. Ashhab, Y. Wu, and F. Nori, Sci. Rep. **3**, 2943 (2013).

[25] K. Stannigel, P. Komar, S. J. M. Habraken, S. D. Bennett, M. D. Lukin, P. Zoller, and P. Rabl, Phys. Rev. Lett. **109**, 013603 (2012).

[26] P. Kómár, S. D. Bennett, K. Stannigel, S. J. M. Habraken, P. Rabl, P. Zoller, and M. D. Lukin, Phys. Rev. A **87**, 013839 (2013).

[27] M. Ludwig, A. H. Safavi-Naeini, O. Painter, and F. Marquardt, Phys. Rev. Lett. **109**, 063601 (2012).

[28] F. Massel, S. U. Cho, J.-M. Pirkkalainen, P. Hakonen, T. T. Heikkilä, and M. A. Sillanpää, Nat. Commun. **3**, 987 (2012).

[29] H. Seok, L. F. Buchmann, E. M. Wright, and P. Meystre, Phys. Rev. A **88**, 063850 (2013).

[30] L. F. Buchmann and D. M. Stamper-Kurn, Phys. Rev. A **92**, 013851 (2015).

[31] G. Heinrich and F. Marquardt, Europhys. Lett. **93**, 18003 (2011).

[32] J. R. Johansson, G. Johansson, and F. Nori, Phys. Rev. A **90**, 053833 (2014).

[33] T. T. Heikkilä, F. Massel, J. Tuorila, R. Khan, and M. A. Sillanpää, Phys. Rev. Lett. **112**, 203603 (2014).

[34] A. J. Rimberg, M. P. Blencowe, A. D. Armour, and P. D. Nation, New J. Phys. **16**, 055008 (2014).

[35] X.-Y. Lü, Y. Wu, J. R. Johansson, H. Jing, J. Zhang, and F. Nori, Phys. Rev. Lett. **114**, 093602 (2015).

[36] X.-Y. Lü, J.-Q. Liao, L. Tian, and F. Nori, Phys. Rev. A **91**, 013834 (2015).

[37] M.-A. Lemonde, N. Didier, and A. A. Clerk, Nat. Commun. **7**, 11338 (2016).

[38] T.-S. Yin, X.-Y. Lü, L.-L. Zheng, M. Wang, S. Li, and Y. Wu, Phys. Rev. A **95**, 053861 (2017).

[39] M. Ludwig and F. Marquardt, Phys. Rev. Lett. **111**, 073603 (2013).

[40] L.-L. Wan, X.-Y. Lü, J.-H. Gao, and Y. Wu, Opt. Express **25**, 17364 (2017).

[41] J. H. Gan, H. Xiong, L.-G. Si, X.-Y. Lü, and Y. Wu, Opt. Lett. **41**, 2676 (2016).

[42] J. D. Thompson, B. M. Zwickl, A. M. Jayich, F. Marquardt, S. M. Girvin, and J. G. E. Harris, Nature (London) **452**, 72 (2008).

[43] J. C. Sankey, C. Yang, B. M. Zwickl, A. M. Jayich, and J. G. E. Harris, Nat. Phys. **6**, 707 (2010).

[44] M. Bhattacharya, H. Uys, and P. Meystre, Phys. Rev. A **77**, 033819 (2008).

[45] A. Xuereb and M. Paternostro, Phys. Rev. A **87**, 023830 (2013).

[46] J.-Q. Liao and F. Nori, Phys. Rev. A **88**, 023853 (2013).

[47] L.-G. Si, H. Xiong, M. S. Zubairy, and Y. Wu, Phys. Rev. A **95**, 033803 (2017).

[48] M. R. Vanner, Phys. Rev. X **1**, 021011 (2011).

[49] X.-Y. Lü, G.-L. Zhu, L.-L. Zheng, and Y. Wu, Phys. Rev. A **97**, 033807 (2018).

[50] M. Eichenfield, J. Chan, R. M. Camacho, K. J. Vahala, and O. Painter, Nature (London) **462**, 78 (2009).

[51] A. G. Krause, J. T. Hill, M. Ludwig, A. H. Safavi-Naeini, J. Chan, F. Marquardt, and O. Painter, Phys. Rev. Lett. **115**, 233601 (2015).

[52] A. H. Safavi-Naeini, T. P. Mayer Alegre, M. Winger, and O. Painter, Appl. Phys. Lett. **97**, 181106 (2010).

[53] K. Vahala, Nature (London) **424**, 839 (2003).

[54] T. J. Kippenberg, S. M. Spillane, and K. J. Vahala, Phys. Rev. Lett. **93**, 083904 (2004).

[55] F.-Y. Hong and S.-J. Xiong, Phys. Rev. A **78**, 013812 (2008).

[56] Z.-L. Xiang, S. Ashhab, J.-Q. You, and F. Nori, Rev. Mod. Phys. **85**, 623 (2013).

[57] J.-Q. You and F. Nori, Nature (London) **474**, 589 (2011); Phys. Today **58**(11), 42 (2005).

[58] E. J. Kim, J. R. Johansson, and F. Nori, Phys. Rev. A **91**, 033835 (2015).

[59] M. Bhattacharya and P. Meystre, Phys. Rev. Lett. **99**, 073601 (2007).

[60] A. F. Pace, M. J. Collett, and D. F. Walls, Phys. Rev. A **47**, 3173 (1993).

[61] D. Vitali, S. Gigan, A. Ferreira, H. R. Böhm, P. Tombesi, A. Guerreiro, V. Vedral, A. Zeilinger, and M. Aspelmeyer, Phys. Rev. Lett. **98**, 030405 (2007).

[62] I. Wilson-Rae, N. Nooshi, W. Zwerger, and T. J. Kippenberg, Phys. Rev. Lett. **99**, 093901 (2007).

[63] F. Marquardt, J. P. Chen, A. A. Clerk, and S. M. Girvin, Phys. Rev. Lett. **99**, 093902 (2007).

[64] M.-A. Lemonde and A. A. Clerk, Phys. Rev. A **91**, 033836 (2015).

[65] Our numerical results on the phonon sideband and photon blockade are calculated based on the QuTiP package [J. R. Johansson, P. D. Nation, and F. Nori, Comput. Phys. Commun. **183**, 1760 (2012); **184**, 1234 (2013)].

[66] J. Chan, M. Eichenfield, R. M. Camacho, and O. Painter, Opt. Express **17**, 3802 (2009); J. Chan, A. H. Safavi-Naeini, J. T. Hill, S. Meenehan, and O. Painter, Appl. Phys. Lett. **101**, 081115 (2012).

[67] K. W. Murch, K. L. Moore, S. Gupta, and D. M. StamperKurn, Nat. Phys. **4**, 561 (2008).